FLIGHT PATH RECONSTRUCTION USING THE UNSCENTED KALMAN FILTER ALGORITHM

Bruno Otávio Soares Teixeira
Centro de Pesquisa e de Desenvolvimento em Engenharia Elétrica – Universidade Federal de Minas Gerais
Laboratório de Modelagem, Análise e Controle de Sistemas Não-Lineares (MACSIN)
Av. Antônio Carlos, 6627, 31270-901, Belo Horizonte – MG, Brasil
brunoot@cpdee.ufmg.br

Leonardo Antônio Borges Tôrres
Departamento de Engenharia Eletrônica – MACSIN – Universidade Federal de Minas Gerais
torres@cpdee.ufmg.br

Paulo Henriques Iscold Andrade de Oliveira
Departamento de Engenharia Mecânica – Centro de Estudos Aeronáuticos (CEA) – Universidade Federal de Minas Gerais
iscold@ufmg.br

Luis Antonio Aguirre
Departamento de Engenharia Eletrônica – MACSIN – Universidade Federal de Minas Gerais
aguirre@cpdee.ufmg.br

Abstract. *This paper illustrates the application of the Flight Path Reconstruction procedure to both simulated and real data collected from a sailplane aircraft. In both cases a specific type of Sigma-Point Kalman Filter, known as the Unscented Kalman Filter (UKF), is employed to determine the biases associated to each accelerometer and gyro in the Inertial Measurement Unit (IMU), together with high sampling rate trajectory reconstruction from low frequency sampled GPS data.*

Keywords: *Flight Path Reconstruction, Unscented Kalman Filter, Filter Error Method, GPS and Inertial fusion*

1. Introduction

Currently, there has been much effort towards the use of efficient algorithms to determine aircraft control and stability derivatives, not only from wind tunnel experiments or Computational Fluid Dynamics analysis, but also based on real data collected by onboard instrumentation, during flight tests [Jategaonkar et al., 2004, Jategaonkar and Thielecke, 2002].

The problem of Flight Path Reconstruction (FPR) is the first step in the procedure of using flight tests data to obtain information about the parameters of the aircraft model [Mulder et al., 1999]. Roughly, this reconstruction means the estimation of aircraft trajectory, based on aircraft sensors data. This step is crucial and fundamental, because real sensors do present bias and sensitivity mismatches that must be accounted for in the subsequent phases of the analysis. Estimated values for bias and sensitivity terms can be obtained in the process of flight trajectory reconstruction.

Output-error and filter-error methods [Mendonça et al., 2004, Mulder et al., 1999, Jategaonkar et al., 2004] have been used to solve the FPR problem. Whereas the former approach only regards about measurement errors, the latter, which is treated in this paper, is also able to deal with process noise (present in the IMU measurements for instance).

The original work on Kalman filtering [Kalman, 1960] gave rise to a very popular approach: the Extended Kalman Filter (EKF) [Haykin, 2001] that relies on linearization in order to propagate the state covariance matrix of the dynamical system. In some cases this can lead to unbounded estimation error estimates. One such instance is observed when the system is described by highly nonlinear equations as in the kinematic analysis of 6 degrees of freedom rigid bodies. Among many alternatives to the EKF, one can highlight the so-called Sigma-Point Kalman Filter (SPKF) and derivatives [van der Merwe et al., 2004] which are based on the propagation of the state covariance matrix using the ensemble statistics generated by suitably chosen points — the *sigma-points* — around the estimated state in the state space.

This paper illustrates the application of the FPR procedure to both simulated and real data collected from a sailplane aircraft. In both cases a specific type of SPKF, known as the Unscented Kalman Filter (UKF) [Julier and Uhlmann, 2004], is employed to determine the biases associated to each accelerometer and gyro in the IMU, together with high sampling rate trajectory reconstruction from low frequency sampled GPS [1] data.

The paper is organized as follows. In Sec. 2, the problem of state vector recursive estimation is presented in this general form. In Sec. 3, the UKF algorithm is presented, together with a smoothing algorithm employed to enhance the state estimation by means of offline computations. The problem of FPR is cast in terms of nonlinear recursive state vector estimation in Sec. 3.2. Simulation results are presented in Sec. 3.3. In Sec. 4, the algorithm is used in a real case. The data was obtained from flight tests on a sailplane aircraft. Finally, the main paper conclusions are presented in Sec. 5.

[1] Global Posistioning System.

2. Problem Description

The state estimation problem for the continuous-time nonlinear dynamical system

$$\begin{cases} \dot{\mathbf{x}}_t = f[\mathbf{x}_t, \mathbf{u}_t, \mathbf{w}_t], \\ \mathbf{y}_t = h[\mathbf{x}_t, \mathbf{r}_t], \end{cases} \tag{1}$$

where $f[\cdot]$ and $h[\cdot]$ are respectively the assumed known process and observation models, can be described as follows. Suppose that the only known data are the initial conditions $\mathbf{x}(0) \in \mathbb{R}^n$, the measurements $\mathbf{y}_t \in \mathbb{R}^m$ and the control inputs $\mathbf{u}_t \in \mathbb{R}^p,\ \forall t > 0$. Process noise $\mathbf{w}_t \in \mathbb{R}^n$ and measurement noise $\mathbf{r}_t \in \mathbb{R}^m$ are assumed white, Gaussian, zero-mean and mutually independent with covariance matrices Q and R, respectively. It is desired to obtain an estimate for the unobserved state vector $\mathbf{x}_t,\ \forall t > 0$.

3. The UKF Algorithm

Many difficulties associated to the EKF have been partially circumvented by the use of the UKF which is based on the intuition that it should be easier to approximate a Gaussian distribution than an arbitrary nonlinear function [Julier et al., 1995]. Instead of linearizing the model equations, this algorithm propagates a small representative group of deterministically chosen points (actually vectors) named sigma points $\mathcal{X}_i,\ i = 0, 1, \ldots, 2n_\mathrm{a}$ (where n_a is the dimension of the augmented state vector) which by construction includes the mean and covariance information of the state estimate at time $k-1$ (with $t = kT_\mathrm{s}$ where k denotes discrete time and T_s is the sampling period) in order to numerically calculate the prior state estimate $\hat{\mathbf{x}}_{k|k-1}$ and its covariance matrix $P_{k|k-1}$ by their propagation through the discrete counterpart of the nonlinear equations (1). Hence, the algorithm can be implemented as follows.

Firstly, an augmented state vector is composed by the concatenation of the original state, process and measurement noise variables thus $\mathbf{x}^\mathrm{a}_k = [\mathbf{x}^\mathrm{T}_k\ \ \mathbf{w}^\mathrm{T}_k\ \ \mathbf{r}^\mathrm{T}_k]^\mathrm{T}$, and $\mathbf{x}^\mathrm{a}_k \in \mathbb{R}^{n_\mathrm{a}}$ where $n_\mathrm{a} = 2n + m$. Consequently the covariance matrix of the vector of estimation errors must refer to this augmented state vector and henceforth it will be referred to as $P^{\,\mathrm{a}} \in \mathbb{R}^{(2n+m)\times(2n+m)}$, that is

$$P^\mathrm{a} = \begin{bmatrix} P & 0 & 0 \\ 0 & Q & 0 \\ 0 & 0 & R \end{bmatrix}. \tag{2}$$

The sigma points can be chosen as

$$\begin{cases} \mathcal{X}^\mathrm{a}_{0,\ k-1|k-1} = \hat{\mathbf{x}}^\mathrm{a}_{k-1|k-1} \\ \mathcal{X}^\mathrm{a}_{i,\ k-1|k-1} = \hat{\mathbf{x}}^\mathrm{a}_{k-1|k-1} + \left[\sqrt{(n_\mathrm{a}+\lambda)P^\mathrm{a}_{k-1|k-1}}\right]_i \\ \mathcal{X}^\mathrm{a}_{i+n_\mathrm{a},\ k-1|k-1} = \hat{\mathbf{x}}^\mathrm{a}_{k-1|k-1} - \left[\sqrt{(n_\mathrm{a}+\lambda)P^\mathrm{a}_{k-1|k-1}}\right]_i, \end{cases} \tag{3}$$

with associated weights given by

$$\begin{cases} w^{(m)}_0 = \frac{\lambda}{n_\mathrm{a}+\lambda} \\ w^{(c)}_0 = \frac{\lambda}{n_\mathrm{a}+\lambda} + 1 - \alpha^2 + \beta \\ w^{(m)}_i = w^{(c)}_i = \frac{1}{2(n_\mathrm{a}+\lambda)}, \end{cases} \tag{4}$$

with $i = 1, \ldots, n_\mathrm{a}$ and $[\sqrt{(\cdot)}]_i$ is either the i th row or column of the matrix square-root [Julier and Uhlmann, 2004]. For the sake of simplicity the following choices are made $\lambda = \alpha^2(\kappa + n_\mathrm{a}) - n_\mathrm{a} = 0$ [Julier and Uhlmann, 2004] $\alpha = 1$, $\kappa = 0$ and $\beta = 2$ [Haykin, 2001]. Choosing the sigma points as indicated in (3) guarantees exact matching of the first three moments. The unscented Kalman filter equations can be expressed as [Julier and Uhlmann, 2004, Haykin, 2001]

$$\begin{cases} \hat{\mathbf{x}}_{k|k-1} = \sum_{i=0}^{2n_\mathrm{a}} w^{(m)}_i \mathcal{X}^x_{i,\ k|k-1}, \quad \text{where} \quad \mathcal{X}^x_{i,\ k|k-1} = f[\mathcal{X}^x_{i,\ k-1|k-1},\ \mathbf{u}_{k-1},\ \mathcal{X}^w_{i,\ k-1|k-1}] \\ \hat{\mathbf{y}}_{k|k-1} = \sum_{i=0}^{2n_\mathrm{a}} w^{(m)}_i \mathcal{Y}_{i,\ k|k-1}, \quad \text{where} \quad \mathcal{Y}_{i,\ k|k-1} = h[\mathcal{X}^x_{i,\ k|k-1},\ \mathcal{X}^r_{i,\ k|k-1}] \\ P_{k|k-1} = \sum_{i=0}^{2n_\mathrm{a}} w^{(c)}_i [\mathcal{X}^x_{i,\ k|k-1} - \hat{\mathbf{x}}_{i,\ k|k-1}][\mathcal{X}^x_{i,\ k|k-1} - \hat{\mathbf{x}}_{i,\ k|k-1}]^\mathrm{T} \\ P^{yy}_{k|k-1} = \sum_{i=0}^{2n_\mathrm{a}} w^{(c)}_i [\mathcal{Y}_{i,\ k|k-1} - \hat{\mathbf{y}}_{i,\ k|k-1}][\mathcal{Y}_{i,\ k|k-1} - \hat{\mathbf{y}}_{i,\ k|k-1}]^\mathrm{T} \\ P^{xy}_{k|k-1} = \sum_{i=0}^{2n_\mathrm{a}} w^{(c)}_i [\mathcal{X}^x_{i,\ k|k-1} - \hat{\mathbf{x}}_{i,\ k|k-1}][\mathcal{Y}_{i,\ k|k-1} - \hat{\mathbf{y}}_{i,\ k|k-1}]^\mathrm{T} \\ K_k = P^{xy}_{k|k-1} \left[P^{yy}_{k|k-1}\right]^{-1}, \end{cases} \tag{5}$$

with $i = 0, \ldots, 2n_\mathrm{a}$ and where $\mathcal{X}^a_{i,\ k-1|k-1}$ are given by (3) and $\mathcal{X}^{\,a} = [(\mathcal{X}^x)^\mathrm{T}\ (\mathcal{X}^w)^\mathrm{T}\ (\mathcal{X}^r)^\mathrm{T}]^\mathrm{T}$. The set of equations (5) forms the *prediction* or *propagation* step of the UKF that propagates the state estimate one step ahead using the process model. In the case of a continuous-time dynamical system, the state estimate at $t = (k-1)T_\mathrm{s}$ (represented by the sigma points $\mathcal{X}^a_{k-1|k-1}$) can be used as initial conditions to numerically integrate equations (1) one step ahead. This way the discrete form of the UKF algorithm can be readily used.

The *updating* or *correction* equations are

$$\begin{cases} \hat{\mathbf{x}}_{k|k} = \hat{\mathbf{x}}_{k|k-1} + K_k[\mathbf{y}_k - h[\hat{\mathbf{x}}_{k|k-1}]] \\ P_{k|k} = P_{k|k-1} - K_k P^{yy}_{k|k-1} K_k^{\mathrm{T}}. \end{cases} \tag{6}$$

In closing this section, it is important to remark that the updating equations of the EKF and UKF filters are the same. The differences between the aforementioned algorithms are found in the prediction step. Whereas the former ignores the statistics of the state estimate $\hat{\mathbf{x}}_{k-1|k-1}$ during the linearization of the model in order to approximate the prior covariance matrix $P_{k|k-1}$, the latter accurately calculates it through the sigma point approach. The UKF achieves second order accuracy (similar to the case of using second-order truncated Taylor series model approximation in the EKF) with equivalent computational costs of the first-order EKF but with easier implementation (Jacobian matrices are no more necessary) [Julier et al., 1995].

For details on Kalman filtering in general, the reader is referred to [Maybeck, 1979, Crassidis and Junkis, 2004] and for the UKF see [Julier and Uhlmann, 2004, Haykin, 2001] and references therein. The use of the UKF in the context of nonlinear dynamics is treated in [Aguirre et al., 2005].

3.1 The UKS Algorithm

In the previous section the UKF was presented as a recursive algorithm that provides estimates of the state vector $\hat{\mathbf{x}}_{k|k}$ based on all past and present measurement vectors $\mathbf{y}_1, \mathbf{y}_2, \ldots, \mathbf{y}_k$. In the case of offline estimation, such as the FPR problem, the Unscented Kalman Smoother (UKS) [Haykin, 2001] may be employed to produce improved estimates (the measurement noise effects are smoothed out further) by the use of future measurements $\mathbf{y}_{k+1}, \mathbf{y}_{k+2}, \ldots, \mathbf{y}_N$, where N equals the total length of the flight test data. To achieve this goal, the UKS optimally combines the results of a foward and a backward UKF. The former estimates mean and covariance $(\hat{\mathbf{x}}^{\mathrm{f}}_{k|k}, P^{\mathrm{f}}_{k|k})$ given past and present data, and the latter estimates $(\hat{\mathbf{x}}^{\mathrm{b}}_{k|k+1}, P^{\mathrm{b}}_{k|k+1})$ given future data. The forward UKF is implemented exactly as shown by equations (5) and (6) whereas the backward UKF can make use of the following backward counterpart continuous-time model before applying the same algorithm:

$$\begin{cases} \dot{\mathbf{x}}_{-t} = -f[\mathbf{x}_{-t}, \mathbf{u}_{-t}, \mathbf{w}_{-t}] \\ \mathbf{y}_{-t} = h[\mathbf{x}_{-t}, \mathbf{r}_{-t}], \end{cases} \tag{7}$$

where $-t$ denotes time inversion of input and output data. The optimal way that the UKS combines the forward and backward filter results in order to produce the smoothed mean and covariance $(\hat{\mathbf{x}}^{\mathrm{s}}_k, P^{\mathrm{s}}_k)$ of the states is given by the following equations

$$\begin{cases} [P^{\mathrm{s}}_k]^{-1} = [P^{\mathrm{f}}_{k|k}]^{-1} + [P^{\mathrm{b}}_{k|k+1}]^{-1} \\ \hat{\mathbf{x}}^{\mathrm{s}}_k = P^{\mathrm{s}}_k \left[[P^{\mathrm{f}}_{k|k}]^{-1} \hat{\mathbf{x}}^{\mathrm{f}}_{k|k} + [P^{\mathrm{b}}_{k|k+1}]^{-1} \hat{\mathbf{x}}^{\mathrm{b}}_{k|k+1} \right]. \end{cases} \tag{8}$$

When it comes to online applications, the iterative Kalman filter may reduce the effect of observation equation nonlinearities (recall that the UKF is a kind of a second-order EKF in terms of accuracy), improving the current state estimate by applying local iterations to repeatedly calculate $\mathbf{x}_{k|k}$, $P_{k|k}$ and K_k.[2] In the case of EKF, the iterative approach requires the local linearization of the observation model in each iteration [Crassidis and Junkis, 2004]. Similarly, in the context of the UKF, new sigma points (3) should be calculated at each iteration, an issue that will be treated in a future paper.

Besides reducing the effect of observation nonlinearities, given that slowly sampled observations — such as the ones provided by some GPS receivers — can be used, the aforementioned approaches somewhat play the role of interpolators, which helps to mitigate the abrupt artificial changes in the position variables that appear in the estimates.

3.2 FPR and the UKF algorithm

In the FPR problem, kinematic models are used to describe the temporal evolution of a six degrees of freedom rigid body. These equations consists of three sets of nonlinear first-order ordinary differential equations (ODE) as follows. The first set describe how the translational velocity components u, v and w, along the rigid body axes, evolves with time:

$$\begin{cases} \dot{u} = -q\, w \;+\; r\, v \;-\; g\, \sin\theta \;+\; A_x, \\ \dot{v} = -r\, u \;+\; p\, w \;+\; g\, \cos\theta\, \sin\phi \;+\; A_y, \\ \dot{w} = -p\, v \;+\; q\, u \;+\; g\, \cos\theta\, \cos\phi \;+\; A_z. \end{cases} \tag{9}$$

The second set accounts for the rotational dynamics through the time histories of the Euler angles ϕ, θ and ψ with respect to the earth-fixed reference frame:

$$\begin{cases} \dot{\phi} = -p \;+\; q\, \sin\phi\, \tan\theta \;+\; r\, \cos\phi\, \tan\theta, \\ \dot{\theta} = q\, \cos\phi \;-\; r\, \sin\phi, \\ \dot{\psi} = q\, \sin\phi\, \sec\theta \;+\; r\, \cos\phi\, \sec\theta. \end{cases} \tag{10}$$

[2] According to [Mulder et al., 1999] four to eight iterations are generally employed in FPR.

Finally, numerically integrating the following set of navigation ODE together with the force (9) and the attitude equations (10) the position of the aircraft's c.g. (x_E, y_E, H) relative to the earth-fixed reference may be determined:

$$\begin{bmatrix} \dot{x}_E \\ \dot{y}_E \\ \dot{H} \end{bmatrix} = L_{B2E} \begin{bmatrix} u \\ v \\ w \end{bmatrix} + \begin{bmatrix} W_{x_E} \\ W_{y_E} \\ W_H \end{bmatrix}, \tag{11}$$

where the orthogonal matrix L_{B2E} relates the rigid body and the fixed-earth reference frames

$$L_{B2E} = \begin{bmatrix} \cos\theta\,\cos\psi & \sin\phi\,\sin\theta\,\cos\psi - \cos\phi\,\sin\psi & \cos\phi\,\sin\theta\,\cos\psi + \sin\phi\,\sin\psi \\ \cos\theta\,\sin\psi & \sin\phi\,\sin\theta\,\sin\psi + \cos\phi\,\cos\psi & \cos\phi\,\sin\theta\,\sin\psi - \sin\phi\,\cos\psi \\ -\sin\theta & \sin\phi\,\cos\theta & \cos\phi\,\cos\theta \end{bmatrix}, \tag{12}$$

and W_{x_E}, W_{y_E} and W_H account for the components of a generally assumed constant atmospheric wind vector along the earth-fixed reference frame. At this point, it is important to emphasize that Equations (9), (10) and (11) form the nonlinear kinematic *process* model of an airplane (or any rigid body) in state space, where the states $\mathbf{x}_t \in \mathbb{R}^9$ are given by

$$\mathbf{x}_t = [u \;\; v \;\; w \;\; \phi \;\; \theta \;\; \psi \;\; x_E \;\; y_E \;\; H]^{\mathrm{T}}, \tag{13}$$

and the aerodynamic forces and the angular rates play the role of inputs $\mathbf{u}_k \in \mathbb{R}^6$ as

$$\mathbf{u}_k = [A_{x,\mathrm{m}} \;\; A_{y,\mathrm{m}} \;\; A_{z,\mathrm{m}} \;\; p_{\mathrm{m}} \;\; q_{\mathrm{m}} \;\; r_{\mathrm{m}}]^{\mathrm{T}}. \tag{14}$$

where the subscript m identifies that the variable is measured by onboard intrumentation. The state space dynamical model is completed by considering the *observation* equations whose measurement vector $\mathbf{y}_k \in \mathbb{R}^9$ can be compound by the following variables

$$\mathbf{y}_k = [\phi_{\mathrm{m}} \;\; \theta_{\mathrm{m}} \;\; \psi_{\mathrm{m}} \;\; V_{TAS,\mathrm{m}} \;\; \alpha_{\mathrm{m}} \;\; \beta_{\mathrm{m}} \;\; x_{E,m} \;\; y_{E,m} \;\; H_{\mathrm{m}}]^{\mathrm{T}}, \tag{15}$$

with the Euler angles ϕ_{m}, θ_{m} and ψ_{m} also generally given by the IMU, $V_{TAS,\mathrm{m}}$ is the true airspeed measured directly by means of an annemometer or a Pitot tube system, α_{m} and β_{m} are respectively the attack and sideslip angles measured by vanes, $x_{E,m}$ and $y_{E,m}$ are the geographical coordinates provided by GPS receivers and H refers to the altitude (or the z_E position coordinate in the fixed-earth frame) given by barometric sensors.

Thus the complete state space dynamical model (1) of an aircraft used in FPR can be given by

$$\dot{\mathbf{x}}_t = f[\mathbf{x}_t, \mathbf{u}_{kT_{\mathrm{s}}}, \mathbf{w}_{kT_{\mathrm{s}}}] = \begin{bmatrix} -(q_{\mathrm{m}} - \Delta_q)w + (r_{\mathrm{m}} - \Delta_r)v - g\sin\theta + (A_{x,\mathrm{m}} - \Delta_{A_x}) \\ -(r_{\mathrm{m}} - \Delta_r)u + (p_{\mathrm{m}} - \Delta_p)w + g\cos\theta\sin\phi + (A_{y,\mathrm{m}} - \Delta_{A_y}) \\ -(p_{\mathrm{m}} - \Delta_p)v + (q_{\mathrm{m}} - \Delta_q)u + g\cos\theta\cos\phi + (A_{z,\mathrm{m}} - \Delta_{A_z}) \\ (p_{\mathrm{m}} - \Delta_p) + (q_{\mathrm{m}} - \Delta_q)\sin\phi\tan\theta + (r_{\mathrm{m}} - \Delta r)\cos\phi\tan\theta \\ (q_{\mathrm{m}} - \Delta_q)\cos\phi - (r_{\mathrm{m}} - \Delta_r)\sin\phi \\ (q_{\mathrm{m}} - \Delta_q)\sin\phi\sec\theta + (r_{\mathrm{m}} - \Delta_r)\cos\phi\sec\theta \\ [L_{B2E}]_1\, u + W_{x_E} \\ [L_{B2E}]_2\, v + W_{y_E} \\ [L_{B2E}]_3\, w + W_H \end{bmatrix} + \begin{bmatrix} w_u \\ w_v \\ w_w \\ w_\phi \\ w_\theta \\ w_\psi \\ w_{x_E} \\ w_{y_E} \\ w_H \end{bmatrix}, \tag{16}$$

$$\mathbf{y}_k = h[\mathbf{x}_{\frac{t}{T_{\mathrm{s}}}}, \mathbf{r}_k] = \begin{bmatrix} K_\phi\phi + \Delta_\phi \\ K_\theta\theta + \Delta_\theta \\ K_\psi\psi + \Delta_\psi \\ K_V\sqrt{u^2+v^2+w^2} + \Delta_{V_T} \\ K_\alpha \arctan\left(\frac{w}{u}\right) + \Delta_\alpha \\ K_\beta \arctan\left(\frac{v}{\sqrt{u^2+w^2}}\right) + \Delta_\beta \\ K_{x_E}x_E + \Delta_{x_E} \\ K_{y_E}y_E + \Delta_{y_E} \\ K_H H + \Delta_H \end{bmatrix} + \begin{bmatrix} r_{\phi_{\mathrm{m}}} \\ r_{\theta_{\mathrm{m}}} \\ r_{\psi_{\mathrm{m}}} \\ r_{V_{TAS,m}} \\ r_{\alpha_{\mathrm{m}}} \\ r_{\beta_{\mathrm{m}}} \\ r_{x_{E,m}} \\ r_{y_{E,m}} \\ r_{H_{\mathrm{m}}} \end{bmatrix}, \tag{17}$$

where the *measured* inputs $\mathbf{u}_k$ (14) discounts the respective bias (indicated as Δ_{u}, u refers to all components of $\mathbf{u}_k$) in equations (16) whereas all outputs $\mathbf{y}_k$ (15) regards about it (Δ_{y}, y refers to all components of $\mathbf{y}_k$) in (17) besides related scale factors (given by K_{y}, y substitutes all elements of the vector $\mathbf{y}_k$), and both process and measurement noise vectors, $\mathbf{w}_k$ and $\mathbf{r}_k$, are assumed additive, and $[L_{B2E}]_i$ is the ith row of the matrix L_{B2E}.

And last but not least, since the UKF algorithm can be also readily used to jointly estimate system parameters, it is easy to consider a parameter as a "virtual" state. Thus equations (16) can be extended so as to take into account the bias and scale factor effects. In this paper only bias variables are jointly estimated. Although, at first sight, this approach seems simplistic it was successfully employed in [Mulder et al., 1999, van der Merwe et al., 2004]. Moreover

too many parameters may lead to nonreconstructible componentes in the extended state vector. Therefore vector (13) can be concatenated with $\theta_t \in \mathbb{R}^{n_\theta}$

$$\theta_t = \left[\Delta_{A_x}\ \ \Delta_{A_y}\ \ \Delta_{A_z}\ \ \Delta_p\ \ \Delta_q\ \ \Delta_r\ \ \Delta_\phi\ \ \Delta_\theta\ \ \Delta_\psi\ \ \Delta_{V_T}\ \ \Delta_\alpha\ \ \Delta_\beta\ \ \Delta_{x_E}\ \ \Delta_{y_E}\ \ \Delta_H\right]^{\mathrm{T}}, \tag{18}$$

so that $\mathbf{x}_{ext,t} = \left[\mathbf{x}_t^{\mathrm{T}}\ \ \theta_t^{\mathrm{T}}\right]^{\mathrm{T}}$ and equations (16) can by extended by

$$\dot{\theta}_t = -\frac{1}{\tau}\theta_t + \mathbf{w}_{\theta,t}, \tag{19}$$

where τ is the correlation time that governs the temporal evolution of the parameters θ according to a zero-mean stationary first-order Markov process [Mulder et al., 1999]. Taking τ to infinity, the parameter dynamics is modelled as a random walk sthocastic process that is able to deal with non-zero mean and non-stationary behaviour of some IMU sensors for instance [van der Merwe et al., 2004].

Often it is expected that the system parameters do not vary or, if they do, the variation is much slower than that of the original system state. Then, in both cases, the parameter covariance matrix $Q_\theta \in \mathbb{R}^{n_\theta \times n_\theta}$ of the Gaussian, zero-mean and white-noise random variables $\mathbf{w}_\theta$ accounts for the uncertainty in the estimated parameters and permit their variation with time. [3] Lower-bounding the parameter error covariance matrix P_θ by suitably setting a non-null Q_θ allows to emphasize the most recent data $\mathbf{y}_k$ preventing the algorithm from stalling.

The FPR problem is reviewed in [Mulder et al., 1999]. In [van der Merwe et al., 2004], using a UAV (helicopter) test platform, it is indicated the superior performance of the UKF, when compared to the EKF, with easier implementation and equivalent computational costs.

3.3 Simulation Results

This section reports some tests conducted with simulated data obtained by the FDC toolbox [Rauw, 2005]. This Simulink toolbox models a DHC-2 Beaver aircraft by coupling aerodymanic, atmospheric, gravity and propulsion engine equations in a flat-earth nonlinear state space dynamic model. The states, inputs and outputs are given by equations (13), (14) and (15) respectivelly.

The FPR problem discussed in Sec. 3.2 is treated here by investigating two types of trajectories. Both very rapid and smoother maneuvers are shown in Fig. 1. It is important to note that the very rapid maneuver shown in Fig. 1.a is likely to be unfeasible for the appointed simulation time span of 60s, due to aircraft physical constraints. However, this data set was important to reveal best practices in conducting flight tests, particularly related to sensors parameters estimation.

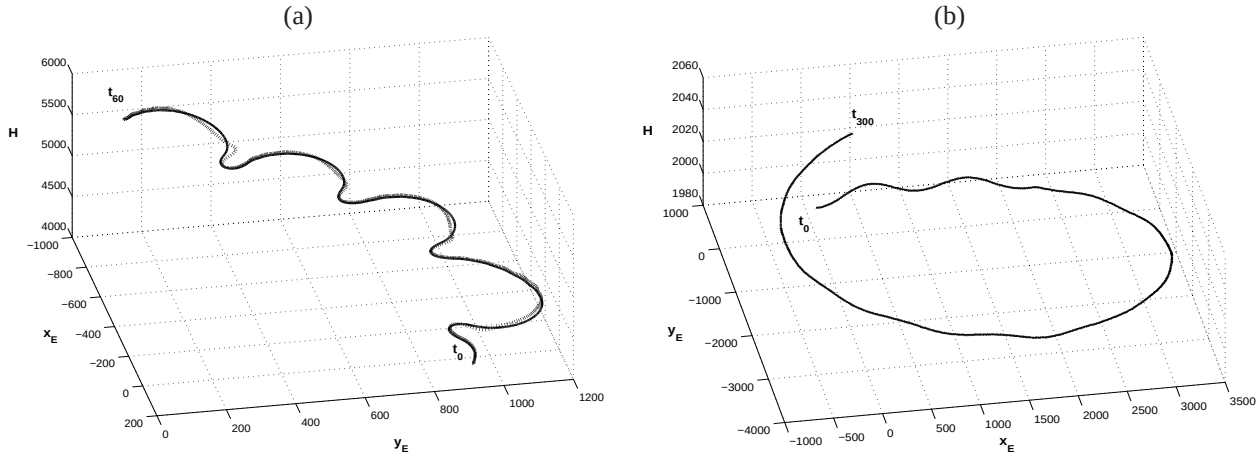

Figure 1. Simulated (—) and reconstructed (. . .) Beaver trajectories: (a) the very rapid one was obtained integrating model equations at $\delta t = 0.005$s during 60s whereas (b) for the smoother it was used $\delta t = 0.01$s during 300s. In both cases the reconstruction considered $T_s = 0.10s$ for all inputs and outputs, except for the GPS measurements ($T_{GPS} = 1.0s$).

Indeed, as can be inferred from the values in Tables 1 and 2, if the initial goal is to estimate bias from the IMU sensors, one should employ data sets corresponding to smooth maneuvers. This seems to be consistent with the fact that steady state flight conditions are more adequate to reveal the effect of accelerometers and gyro biases, because in those cases these mismatches rapidly lead to large errors that can be detected easier than those observed in very rapid and oscillating maneuvers. Despite this, the state estimation errors for the smooth maneuver case reveal that the algorithm is relatively

[3] The greater is the trace of Q_θ, the quicker are the permited variations in θ. Different approaches, namely, fixed or time-varying Q_θ, can be used to tune UKF convergence rate and parameters tracking performance [Haykin, 2001]. For the sake of simplicity, in the present work Q_θ will be taken as a constant matrix.

Table 1. Root mean square (RMS) and normalized RMS (in italic) errors of estimated states for Beaver simulated data (both smooth and rapid trajectories) regarding different signal-to-noise ratios (SNR) in inputs and outputs.

Traj./SNR	$u\,(m/s)$ (%)	$v\,(m/s)$ (%)	$w\,(m/s)$ (%)	$\phi\,(rad)$ (%)	$\theta\,(rad)$ (%)	$\psi\,(rad)$ (%)	$x_E\,(m)$ (%)	$y_E\,(m)$ (%)	$H\,(m)$ (%)
Smooth 1%	0.0015	0.0027	0.0004	0.0001	0.0001	0.1404	3.4426	3.8446	0.1405
	0.0034	*0.0711*	*0.0059*	*0.0810*	*0.0258*	*4.4705*	*0.1081*	*0.0844*	*0.0068*
Rapid 1%	1.7514	1.2325	3.0175	0.0096	0.0016	1.4469	12.6520	20.3046	24.8081
	0.9407	*2.2962*	*2.5933*	*0.5378*	*0.2293*	*46.1579*	*1.3721*	*2.0470*	*0.4264*
Smooth 10%	0.0088	0.0164	0.0034	0.0008	0.0003	0.2811	12.6279	13.1645	0.6067
	0.0201	*0.4364*	*0.0499*	*0.4826*	*0.1949*	*8.9474*	*0.3966*	*0.2890*	*0.0295*
Rapid 10%	3.3807	2.5387	4.7160	0.0159	0.0152	1.3823	50.6492	67.0234	184.6727
	1.8159	*4.7297*	*4.0530*	*0.8902*	*2.1603*	*44.0972*	*5.4928*	*6.7568*	*3.1743*
Smooth 25%	0.0183	0.0380	0.0082	0.0019	0.0008	0.2017	16.0906	17.6577	0.9390
	0.0418	*1.0080*	*0.1195*	*1.1033*	*0.4581*	*6.4217*	*0.5053*	*0.3877*	*0.0456*
Rapid 25%	11.3401	2.5624	10.4396	0.0334	0.0396	1.4381	37.6388	49.0660	207.5675
	6.0910	*4.7739*	*8.9721*	*1.8631*	*5.6101*	*45.8782*	*4.0818*	*4.9465*	*3.5679*

Table 2. Normalized steady-state errors of estimated IMU bias for Beaver simulated data (smooth case only) regarding different noise levels in model inputs and outputs. The following choices were made for bias values: $\Delta_{a_x} = 0.01g$, $\Delta_{a_y} = -0.05g$, $\Delta_{a_z} = -0.02g$, $\Delta_p = 0.5^\circ/s$, $\Delta_q = -0.5^\circ/s$ and $\Delta_r = 0.5^\circ/s$.

SNR	Δ_{a_x} (%)	Δ_{a_y} (%)	Δ_{a_z} (%)	Δ_p (%)	Δ_q (%)	Δ_r (%)
1%	1.0896	-0.1798	3.1236	-0.0016	0.0129	0.1030
10%	1.1864	2.7973	3.9169	0.2442	-0.1767	-3.4034
25%	0.9622	-3.8705	2.0931	-0.7857	0.0858	4.6997

robust to noise in the IMU sensors. The state estimation errors are small, as shown in Table 1 (below 10% even in the worst case) for noise levels ranging from 1% to 25% in the signals provided by the IMU and by the outputs (15).

For the rapid maneuver, the state estimation error worst case was observed for ψ. This seems to be due to the artificial discontinuity introduced when the yaw angle traverses the 2π boundary. This is another strong indication that one should employ quaternions [Stevens and Lewis, 1992], instead of Euler angles, to estimate rigid body attitude.

The results obtained for sensors biases estimation are shown in Table 2. No convergence was obtained for the rapid maneuver case. Two different approaches were used to model the parameters dynamics, as indicated in Equation (19): Markovian ($0 < \tau < \infty$) and random-walk ($\tau \to \infty$) strategies. Only results for the latter approach are presented, although it is important to remark that similar results were observed in both cases.

4. Experimental Data – Sailplane Aircraft

In order to verify the efficiency of the UKF in a real case, the procedure described in Sec. 3 was employed to estimate states and parameters from data collected in flight tests conducted on a SZD 50-3 Puchacz sailplane [PZL-Bielsko, 2005] (see Figure 2). This aircraft is manufactured in fiberglass, with 16.67m wingspan and empty weight of 3600N. The flight test data were obtained during a campaign performed by the Centro de Estudos Aeronáuticos – CEA/UFMG [Centro de Estudos Aeronáuticos – CEA, 2005] in partnership with the Instituto Tecnológico de Aeronáutica - ITA.

The Flight Data Acquisition System – FDAS; i.e. the onboard instrumentation; was developed in the CEA/UFMG and comprises an airdata probe capable of measuring static and dynamic pressures, and angles of attack and sideslip; and accompanying sensors to measure outside air temperature, flight controls positions, and aircraft accelerations using MEMS[4] accelerometers. The angular velocities and translational accelerations were provided by a MicroStrain 3DM-GX1 IMU, which was connected to a portable computer. The inertial data collected using the commercial IMU was properly synchronized with the rest of the acquired data collected using the FDAS-CEA system by means of the MEMS accelerometers signals. Details on the FDAS can be found in [Centro de Estudos Aeronáuticos – CEA, 2005].

The maneuvers were planned to properly excite the aircraft longitudinal (phugoid and short period) and lateral-directional modes. Time series for the estimated attitude and translational velocities are shown in Fig. 3.

In Table 3 real results obtained from the Puchacz sailplane aircraft flight tests data are presented. The percentual errors in the translational velocities were obtained considering that the variables V_T, α and β were perfectly measured, i.e. the airdata probe was considered our calibration standard. In the same way, the attitude information, that was provided by the commercial IMU, and the low frequency GPS data were assumed to be perfect measurements.

The results reveal that the UKS procedure can be effectively used to improve the estimation of high frequency sampled

[4]Microelectromechanical devices.

(a) (b)

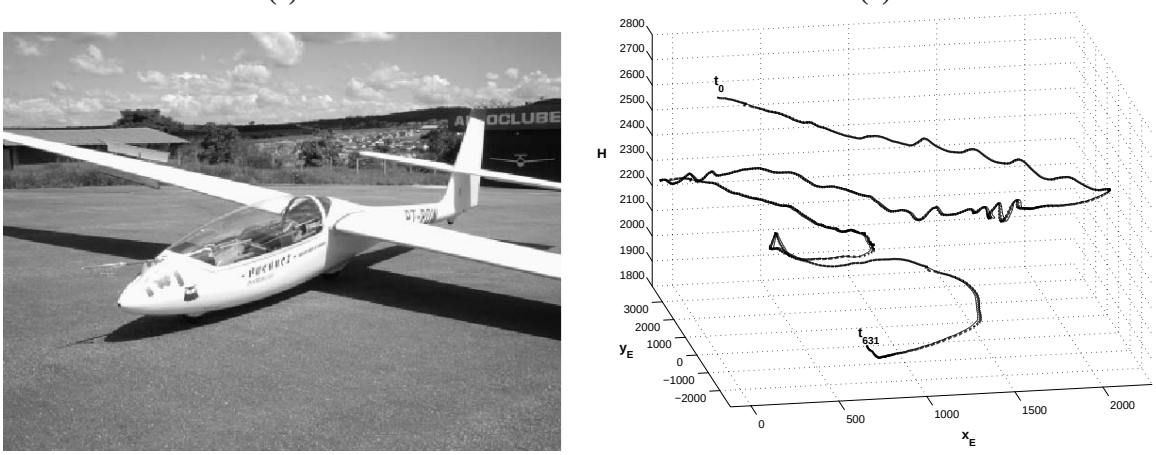

Figure 2. (a) SZD 50-3 Puchacz sailplane. (b) Measured (—) and reconstructed (. . .) aircraft trajectories. Recall that the solid and the dotted lines are overlapped. The flight path reconstruction considered $T_s = 0.10\text{s}$ for all inputs and outputs, except for the GPS measurements ($T_{GPS} = 1.0\text{s}$).

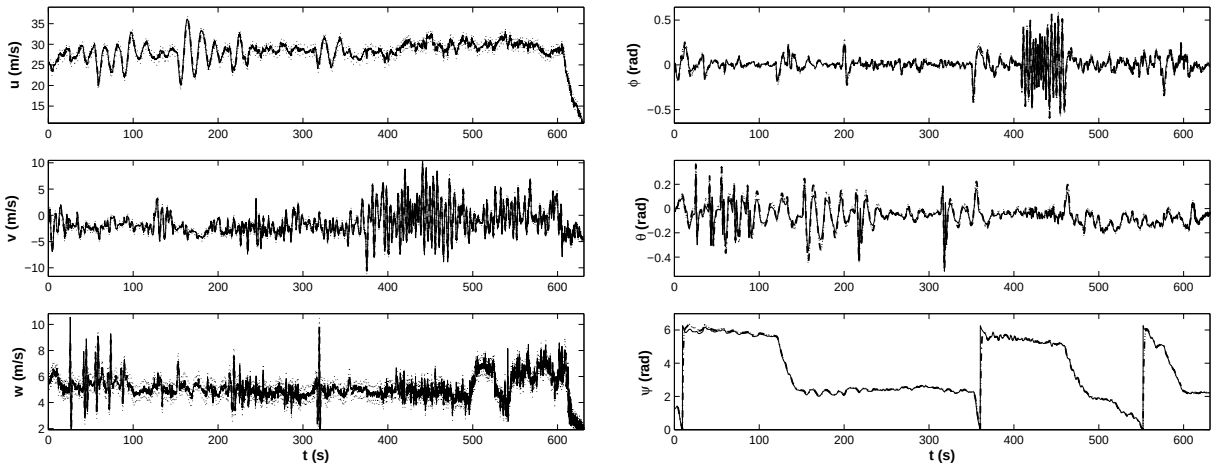

Figure 3. Measured (—) and UKF joint estimated (-··-) velocity componentes (u, v e w) and Euler angles (ϕ, θ e ψ) of SZD 50-3 Puchacz sailplanes's trajectory shown in Figure 2. It is important to note the discontinuity on ψ.

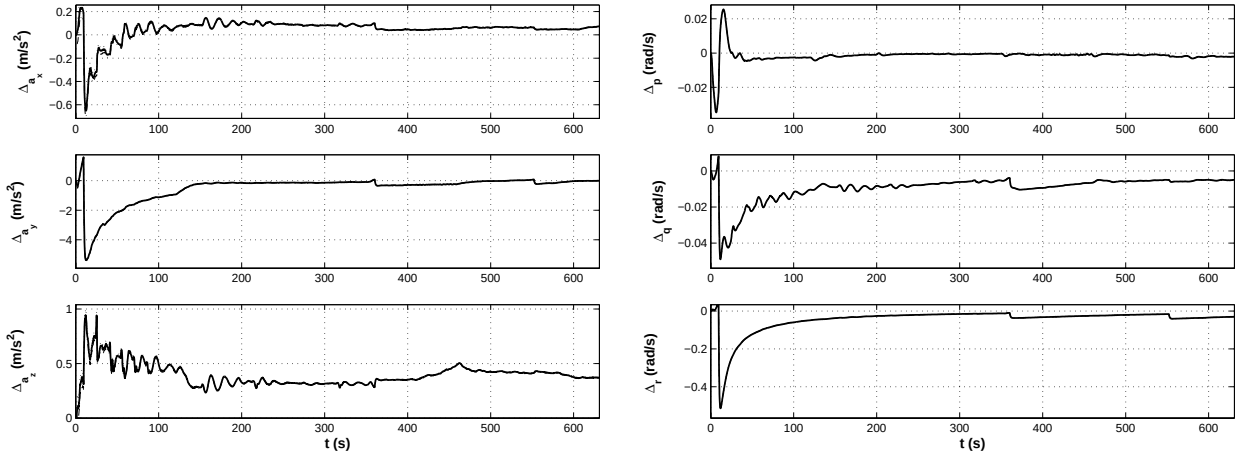

Figure 4. UKF joint estimated IMU sensor biases of SZD 50-3 Puchacz sailplane.

data from low frequency sampled acquired data (GPS measurements), which seems to be consistent with the discussion in Sec. 3.1. When compared to the UKF, the UKS reduced the performance index (RMS error) by a factor of two for high frequency data and by four for the GPS data approximately.

Based on the apparently small values observed for the state estimation errors, it seems that the results obtained for sensor biases estimation, shown in Fig. 4, could be regarded as good approximations of the real sensors parameters. However, it was not possible to validate this conclusion once there was no independent account for the sensor biases.

Table 3. RMS and normalized RMS (in italic) errors of estimated states for Puchacz data for UKF and UKS algorithms.

Traj./SNR	$u\,(m/s)$ (%)	$v\,(m/s)$ (%)	$w\,(m/s)$ (%)	$\phi\,(rad)$ (%)	$\theta\,(rad)$ (%)	$\psi\,(rad)$ (%)	$x_E\,(m)$ (%)	$y_E\,(m)$ (%)	$H\,(m)$ (%)
UKF	0.3685	0.2758	0.1897	0.0224	0.0274	0.2622	10.5580	11.8034	1.0979
	1.0203	*2.6481*	*1.7978*	*4.4328*	*5.3115*	*4.1836*	*0.5126*	*0.3389*	*0.0389*
UKS	0.2136	0.1412	0.1079	0.0149	0.0111	0.0964	2.5140	3.3916	0.4935
	0.5914	*1.3548*	*1.0228*	*2.9335*	*2.1569*	*3.0689*	*0.1220*	*0.0973*	*0.0174*

5. Concluding Remarks

In this paper a Kalman Filter like algorithm – known as the Unscented Kalman Filter – UKF was presented as a viable alternative to perform Flight Path Reconstruction without relying on kinematic equations linearization.

Together with the aforementioned algorithm, a derivated smoothing procedure was also presented. This procedure leads to the Unscented Kalman Smoother (Sec. 3.1), which can be used to enhance the quality of the estimation by combining past and future data in offline calculations to generate smoother high frequency sampled trajectory reconstruction from low frequency GPS data.

As discussed in Sec. 3.3, the flight tests should be conducted so that slowling varying or even static measurements from the onboard sensors are obtained, in order to facilitate the estimation of sensors biases.

The UKF algorithm convergence is greatly affected by the initial process and measurement noise covariance matrices. The initial covariance estimate can be obtained from instrumentation technical specfications related to overall accuracy and precision. It is important to note that there exist the possibility of estimating the noise statistics altogether, which is called adaptive filtering. A deeper analysis in this case is under way.

6. Acknowledgements

The authors are grateful to CAPES and CNPq for financial support.

7. References

Aguirre, L. A., Teixeira, B. O. S., and Tôrres, L. A. B. (2005). Using data-driven discrete-time models and the unscented Kalman filter to estimate unobserved variables of nonlinear systems. *Physical Review E*, 72.

Centro de Estudos Aeronáuticos – CEA (2005). Internet site. http://www.demec.ufmg.br/cea.

Crassidis, J. L. and Junkis, J. L. (2004). *Optimal Estimation of Dynamic Systems*. Chapman & Hall/CRC, Boca Raton.

Haykin, S. (2001). *Kalman Filtering and Neural Networks*. Wiley Publishing, New York.

Jategaonkar, R., Fischenberg, D., and von Gruenhagen, W. (2004). Aerodynamic modeling and system identification from flight data - recent applications at DLR. *Journal of Aircraft*, 41(4):681–691.

Jategaonkar, R. and Thielecke, F. (2002). ESTIMA – an integrated software tool for nonlinear parameter estimation. *Aerospace Science and Technology*, 6(8):565–578.

Julier, S. J. and Uhlmann, J. K. (2004). Unscented filtering and nonlinear estimation. *Proceedings of the IEEE*, 92(3):401–422.

Julier, S. J., Uhlmann, J. K., and Durrant-Whyte, H. F. (1995). A new approach for filtering nonlinear systems. In *The Proceedings of the American Control Conference*, pages 1628–1632, Seattle, Washington.

Kalman, R. E. (1960). A new approach to linear filtering and prediction problems. *Transactions of the ASME-Journal of Basic Engineering*, 82:35–45.

Maybeck, P. S. (1979). *Sthocastic Models, Estimation and Control*, volume 1. Academic Press, San Diego.

Mendonça, C. B., Hemerly, E. M., and Curvo, M. (2004). Reconstrução de trajetória de aeronaves com identificação paramétrica em modelo não-linear. In *XV Congresso Brasileiro de Automática*, Gramado – RS, Brasil.

Mulder, J. A., Chu, Q. P., Sridhar, J. K., Breeman, J., and Laban, M. (1999). Non-linear aircraft flight path reconstruction review and new advances. *Progress in Aerospace Sciences*, 35:673–726.

PZL-Bielsko (2005). SZD 50-3 Puchacz – Internet site. http://www.szdusa.com/50.html.

Rauw, M. O. (2005). FDC 1.4 - A Simulink Toolbox for Flight Dynamics and Control Analysis. Technical report, http://home.wanadoo.nl/dutchroll/index.html.

Stevens, B. L. and Lewis, F. L. (1992). *Aircraft Control and Simulation*. John Wiley & sons, Inc.

van der Merwe, R., Wan, E., and Julier, S. (2004). Sigma-point kalman filters for nonlinear estimation and sensor-fusion: Applications to integrated navigation. In *AIAA Guidance, Navigation and Control Conference and Exhibit*, Providence, Rhode Island. AIAA – American Institute of Aeronautics and Astronautics.